Effect of physical and chemical pressure on the superconductivity of cage-type compound $Lu_5Rh_6Sn_{18}$

Chao Xiong [1,*] Cuiying Pei,[1,*] Qi Wang,[1,2] Juefei Wu [1] Yi Zhao [1] Yuyang Jiang,[1]
Changhua Li,[1] Weizheng Cao,[1] Na Yu [1] Lili Zhang,[3] and Yanpeng Qi[1,2,4,†]

[1]*School of Physical Science and Technology, ShanghaiTech University, Shanghai 201210, China*
[2]*ShanghaiTech Laboratory for Topological Physics, ShanghaiTech University, Shanghai 201210, China*
[3]*Shanghai Synchrotron Radiation Facility, Shanghai Advanced Research Institute, Chinese Academy of Sciences, Shanghai 201203, China*
[4]*Shanghai Key Laboratory of High-Resolution Electron Microscopy, ShanghaiTech University, Shanghai 201210, China*

$Lu_5Rh_6Sn_{18}$ is one of the cage-type superconductors with superconducting transition temperature $T_c = 4.12$ K. Here we investigate the effect of pressure on the superconductivity in $Lu_5Rh_6Sn_{18}$ by combining high-pressure electrical transport, synchrotron x-ray diffraction (XRD), and chemical doping. Application of high pressure can enhance both the metallicity and the superconducting transition temperature in $Lu_5Rh_6Sn_{18}$. T_c is found to show a continuous increase reaching up to 5.50 K at 11.4 GPa. Our high-pressure synchrotron XRD measurements demonstrate the stability of the pristine crystal structure up to 12.0 GPa. In contrast, T_c is suppressed after the substitution of La ions in Lu sites, inducing negative chemical pressure. Our study provides valuable insights into the improvement of superconductivity in caged compounds.

I. INTRODUCTION

Cage-type compounds exhibit three-dimensional structures characterized by the presence of spacious atomic cages enclosing comparatively smaller atoms [1–3]. Because of strong electron-phonon coupling and weak structural coupling, the small atoms can "rattle" with large atomic excursions, ultimately leading to a rattling vibration. Three cage-type compounds, namely, Si/Ge clathrates [4], filled skutterudites (RT_4X_{12}) [5–9], and β-pyrochlore oxides [10–12], have been extensively investigated as "rattling-good" materials. These compounds are renowned for a rich variety of properties [6,13–16], such as heavy-fermion behavior, metal-insulator transitions, multipole ordering, and superconductivity.

Ternary stannides $R_5M_6Sn_{18}$ (R = rare earths, M = transition metals) [17–19] can also be categorized as cage-type compounds, and some of them exhibit superconductivity (SC) with the transition temperature $T_c = 4.4$ K (Sc) [20], 4.0 K (Lu) [21], and 3.0 K (Y) [22] when $M = $ Rh. For the normal state, the resistivity $\rho(T)$ of the Lu and Y compounds did not show a typical metallic behavior and exhibited an unusual temperature variation [21,22]. Heat capacity measurements showed that $Sc_5Rh_6Sn_{18}$ and $Lu_5Rh_6Sn_{18}$ have an isotropic superconducting gap [22,23], while $Y_5Rh_6Sn_{18}$ has an anisotropic gap with point nodes [22]. Interestingly, the muon spin relaxation (μSR) experiments indicated that both $Lu_5Rh_6Sn_{18}$ and $Y_5Rh_6Sn_{18}$ exhibit time-reversal symmetry (TRS) breaking in their superconducting state [21,24]. In addition, coexistence of superconductivity and magnetism

was observed in the reentrant superconductors $Tm_5Rh_6Sn_{18}$ ($T_c = 2.20$ K) [25] and $Er_5Rh_6Sn_{18}$ ($T_c = 1.05$ K) [26] with the same crystal structure.

Given the presence of covalently bonded cage-forming frameworks and the rattling motion of the guest atoms, the caged compounds are in principle sensitive to the external conditions. The application of pressure to caged compounds has led to a profound effect on their physical properties, e.g., superconductivity [27,28]. T_c decreases with increasing pressure for most related superconductors, showing a negative pressure coefficient of T_c [29]. Particularly, the positive pressure coefficient observed in $La_3Ru_4Sn_{13}$ [30] and $Sc_5Rh_6Sn_{18}$ [31] with the rate of 0.03 and 0.10 K/GPa, respectively. It should be noted that those high-pressure studies performed at very limited pressure range. It is intriguing to explore whether this improvement can be sustained at higher pressures.

Motivated by the above issues, we systematically investigate the effect of pressure on the related superconductor. We chose $Lu_5Rh_6Sn_{18}$ as a model system and studied the evolution of superconductivity when applying physical pressure. In order to compare the results, we also conducted chemical doping and discussed the effect of negative chemical pressure on the $Lu_5Rh_6Sn_{18}$ superconductor.

II. EXPERIMENTAL DETAILS

Single crystals of $La_xLu_{5-x}Rh_6Sn_{18}$ ($x = 0$, 0.5, and 1) were grown through a normal Sn-flux method [19,24,32]. High-purity Lu shot (99.9%), La shot (99.9%), Rh powder (99.9%), and Sn shot (99.999%) were mixed in the proportion of Lu:La:Rh:Sn = 5-x:x:10:100. The mixture was then loaded into an alumina crucible and then stored in a quartz tube at a glove box under argon atmosphere. The materials were melted

TABLE I. Crystallographic data of $Lu_5Rh_6Sn_{18}$.

Formula	$Lu_4Rh_6Sn_{19}$
Space group	$I4_1/acd$ (no. 142)
Temperature [K]	278.00
Formula per unit cell, Z	8
a, b [Å]	13.6829(3)
c [Å]	27.3503(9)
Unit cell volume, V [Å^3]	5120.6(3)
Calculated density, ρ(g/cm^3)	9.269
2θ range for data collection/°	5.158 to 52.722
Index ranges	$0 \leqslant h \leqslant 120 \leqslant k \leqslant 170 \leqslant l \leqslant 34$
μ/mm^{-1}	37.126
F(000)	12023.0
Collected reflections	1313
Independent reflections	1313
Goodness-of-fit on F^2	1.046
R_1/wR_2, I $\geqslant 2\sigma$(I)	0.0421/0.1138
R_1/wR_2 [all data]	0.0528/0.1209
Largest diff. peak/hole/(e Å^{-3})	2.65/−3.58

together to 1050 °C for about 24 h, held at 1050 °C for about 3 h, and cooled down to 575 °C at a speed of 5 °C/h. The La concentration is limited up to $x = 1$ since impurity phases become apparent with increasing La concentration. The single crystals $La_xLu_{5-x}Rh_6Sn_{18}$ ($x = 0$, 0.5, and 1) have a shiny surface with typical size of $3 \times 2 \times 2$ mm^3.

Phase and quality examinations of the single crystals were performed on Bruker D8 single-crystal x-ray diffractometer (Mo $K\alpha$, $\lambda = 0.71073$ Å) and Bruker D2 powder x-ray diffractometer (Cu $K\alpha$, $\lambda = 1.54056$ Å). Rietveld refinements of the powder XRD pattern were analyzed utilizing the General Structure Analysis System (GSAS-II) [33]. The composition and microstructure of the samples were characterized by a scanning electron microscope (Phenom Pro) equipped with energy-dispersive spectroscopy (EDS).

Electrical resistivity and magnetization measurements from 1.8 to 300 K were achieved using PPMS and MPMS (Quantum Design), respectively. A standard dc four-probe method with Au wires was adopted to gain the electrical resistivity at ambient pressure. The dc magnetization was measured after both zero-field cooling (ZFC) and field cooling (FC) in an applied magnetic field of 10 Oe and the ac magnetic susceptibility was measured at 1000 Hz and with amplitude of 2 Oe at various temperatures.

High-pressure resistivity measurements were performed in a BeCu-type diamond anvil cell (DAC) with 400-μm culet as described elsewhere [27,34]. A cubic BN/epoxy mixture layer was inserted between the BeCu gasket and the electrical leads. Four platinum foils were placed with the sample following the van der Pauw method [35,36]. High-pressure XRD experiments were performed at beamline BL15U of the Shanghai Synchrotron Radiation Facility ($\lambda = 0.6199$ Å). Mineral oil was used as a pressure-transmitting medium. Rietveld refinement was accomplished employing the GSAS-II to determine the structural parameters. Pressure was measured using the ruby luminescence method [37].

TABLE II. Atomic coordinates, occupations, and equivalent isotropic displacement parameters (Å$^2 \times 10^3$) for $Lu_5Rh_6Sn_{18}$. U_{eq} is defined as 1/3 of the trace of the orthogonalized U_{IJ} tensor.

Atom	Site	Occ.	x	y	z	U(eq)
Lu1	32g	1.0	0.63268	0.88658	0.80712	28.9(3)
Rh1	16d	1.0	0.50000	0.75000	0.75313	26.9(7)
Rh2	32g	1.0	0.50095	0.49344	0.62493	26.8(5)
Sn1	32g	1.0	0.50925	0.57568	0.71185	35.5(4)
Sn2	32g	1.0	0.49476	0.57402	0.53794	40.9(7)
Sn3	16f	1.0	0.32629	0.57623	0.62500	41.2(6)
Sn4	16f	1.0	0.67630	0.57370	0.62500	40.4(6)
Sn5	32g	1.0	0.41256	0.33863	0.58089	32.8(3)
Sn6	16e	1.0	0.78794	1.00000	0.75000	53.1(6)
Sn7	8b	1.0	0.50000	0.75000	0.62500	40.8(7)

III. RESULTS

It has been reported that the $Lu_5Rh_6Sn_{18}$ single crystals exhibit a high degree of disorder and twinning [38]. In order to address this issue, single-crystal XRD measurements are performed at room temperature. Using the twinning tool of the program OLEX2 [39,40], the structure was solved with the SHELXT [41] structure solution program using intrinsic phasing and refined with the SHELXL [42] refinement package using least-squares minimization. The details of the structural refinements are displayed in Tables I and II. The detailed process of the refinement and precise description about the disorder of crystal structure were described in the Supplemental Material [43]. The tetragonal structure of $Lu_5Rh_6Sn_{18}$ is depicted in Fig. 1(a). The close relationship of the $Lu_5Rh_6Sn_{18}$-type arrangement with the primitive cubic Remeika $La_3Rh_4Sn_{13}$ prototype has been widely discussed in the literature [44–46]. Both structures exhibit corner-sharing [RhSn$_6$] [Figs. 1(d) and 1(h)] trigonal prismatic arrays, with distorted distorted [RSn$_{12}$] cuboctahedra for $R =$ La, Lu1 atoms [Figs. 1(c) and 1(f)]. A crucial difference between these two prototypes is that condensed cuboctahedra form in $La_3Rh_4Sn_{13}$ infinite columns along the c axis, while in
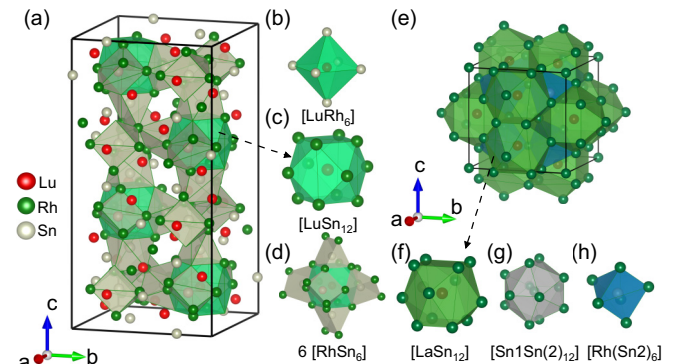
FIG. 1. (a) The crystal structure of $Lu_5Rh_6Sn_{18}$. (b) Distorted octahedra [LuRh$_6$], (c) cuboctahedra [LuSn$_{12}$], and (d) six corner-sharing trigonal prisms [RhSn$_6$] in $Lu_5Rh_6Sn_{18}$. The crystal structure of (e) $La_3Rh_4Sn_{13}$ is also shown here, including (f) cuboctahedra [LaSn$_{12}$], (g) icosahedra [Sn1(Sn2)$_{12}$], and (h) trigonal prisms [Rh(Sn2)$_6$].
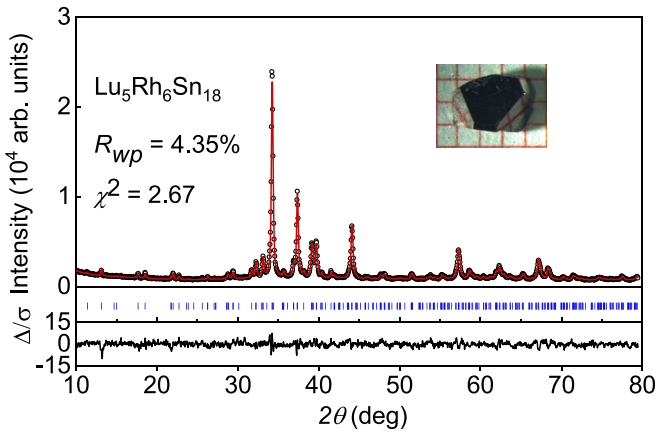
FIG. 2. Powder XRD pattern of $Lu_5Rh_6Sn_{18}$. The solid lines represent the Rietveld fits for $Lu_5Rh_6Sn_{18}$, while the open circles correspond to the observed data. The solid lines at the bottom indicate the residual intensities. The inset shows a photo of the $Lu_5Rh_6Sn_{18}$ single crystals.

the structure of $Lu_5Rh_6Sn_{18}$, they are separated from each other. The interstitial spaces in $La_3Rh_4Sn_{13}$ are filled with ideal $[Sn1Sn(2)_{12}]$ icosahedra [Fig. 1(g)]. Our refined results indicate the existence of Lu atoms in $[LuRh_6]$ are replaced with Sn7 inside cuboctahedras, agreeing well with the EDS measurements (Fig. S2). To check the result analyzed based

on single-crystal XRD, powder XRD measurements were performed on the same batch of $Lu_5Rh_6Sn_{18}$. Figure 2 shows the refined powder XRD pattern of $Lu_5Rh_6Sn_{18}$. The Bragg reflections can be well refined using the obtained structure with reliable parameters. The consistency between powder and single-crystal XRD measurements guarantees the correct phase. The crystal structure of $Lu_5Rh_6Sn_{18}$ exhibits a distortion of a cubic structure (space group Fm-$3m$), resulting in an approximate doubling of the length of the c axis [47]. No trace of superstructure peaks can be observed from the powder XRD pattern, which means the Lu vacancies tend to be randomly distributed in the lattice. Neutron diffraction measurements showcase that there is a significant amount of diffuse scattering, and the weak superlattice reflections are connected by weak diffuse lines [38,48]. Our data, in agreement with neutron diffraction measurements [38], illustrate the highly twinned nature of the crystals, with twin domain scales of 0.53. This indicates the highly twinned nature of the crystals. The disorder of $Lu_5Rh_6Sn_{18}$ may be attributed to a microtwinned stacking disorder of (A, B) square planes [26,47].

Figures 3(a) and S3 show the temperature dependence of the electrical resistivity $\rho(T)$ of $Lu_5Rh_6Sn_{18}$. The normal state of $Lu_5Rh_6Sn_{18}$ exhibits unusual temperature variation: $\rho(T)$ is nearly independent of T down to about 150 K, and shows an increase on further cooling. The negative temperature coefficient of the resistivity ($d\rho/dT < 0$) over a wide temperature
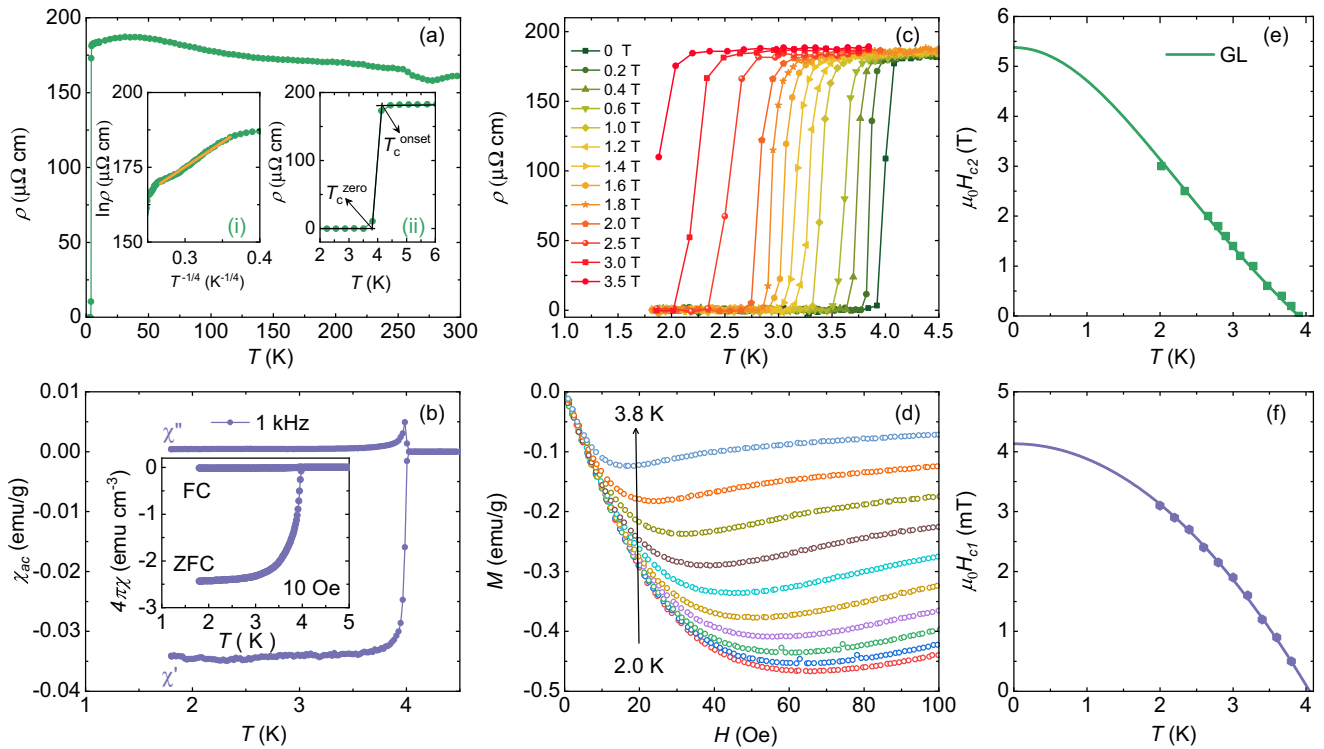
FIG. 3. (a) Resistivity of $Lu_5Rh_6Sn_{18}$ in zero field from 1.8 to 300 K. The inset (i) displays the resistivity data in coordinates $\ln\rho = f(T^{-1/4})$. Yellow line approximates the linear behavior in the temperature range between 60 and 200 K. The inset (ii) illustrates the superconducting transitions at low temperatures. (b) Temperature dependencies of the real and imaginary part of the ac magnetic susceptibility of $Lu_5Rh_6Sn_{18}$. The inset shows the dc magnetic susceptibility in ZFC and FC conditions. (c) Electrical resistivity at various magnetic fields for $Lu_5Rh_6Sn_{18}$. (d) Field dependence of the magnetization $M(H)$ at different temperatures below T_c. (e, f) Temperature dependence of μ_0H_{c2} and μ_0H_{c1} for $Lu_5Rh_6Sn_{18}$.

TABLE III. Superconducting parameters of $Lu_5Rh_6Sn_{18}$ and $LaLu_4Rh_6Sn_{18}$.

	$Lu_5Rh_6Sn_{18}$		$LaLu_4Rh_6Sn_{18}$
	Previous work [54]	This work	This work
T_c^{zero} (K)	4.00	3.90	3.33
T_c^{mag} (K)	–	4.05	3.58
T_c^{onset} (K)	–	4.12	3.72
$\mu_0H_{c2}(0)$ (T)	5.58	5.40	4.30
$\mu_0H_{c1}(0)$ (mT)	4.38	4.14	1.68
$\mu_0H_c(0)$ (mT)	75.0	75.49	39.20
ξ (nm)	7.68	7.81	8.75
λ (nm)	592	415	679
κ	66.8	53.14	77.57

range with $\rho \sim \exp[(\frac{\Delta M}{k_B T})^{1/4}]$ [inset (i) of Fig. 3(a)] is in line with previous reports [49], which is known as the Mott variable-range hopping effect [50,51]. ΔM characterizes the pseudogap in the band structure near the Fermi level. Recently, theoretical calculations for $Lu_5Rh_6Sn_{18}$ documented the pseudogap with very small density of states (DOS) [38], located in the bands of these compounds at a similar binding energy of ~ -0.3 eV. Even a small number of vacancies shifts this pseudogap toward the Fermi level [49]. Our single-crystal XRD measurements demonstrate the existence of Lu vacancies. Therefore the negative temperature coefficient effect in $\rho(T)$ for $Lu_5Rh_6Sn_{18}$ single crystals results from the off-stoichiometry effect.

A sharp superconducting transition occurs at low temperature with a residual resistivity ρ_0 around 181 $\mu\Omega$ cm obtained from extrapolating the normal state to zero temperature. The transition temperatures T_c^{onset} and T_c^{zero} of $Lu_5Rh_6Sn_{18}$ are 4.12 and 3.90 K [inset (ii) of Fig. 3(a)], respectively. Figure 3(b) displays the temperature dependencies of the real (χ') and imaginary (χ'') parts of the ac magnetic susceptibility χ_{ac} of $Lu_5Rh_6Sn_{18}$. The inset shows the dc magnetic susceptibility of $Lu_5Rh_6Sn_{18}$ crystal measured with magnetic field $H = 10$ Oe in ZFC and FC conditions. A clear onset of the diamagnetic shift was observed at $T_c^{\text{mag}} = 4.05$ K, in agreement with the resistivity result. The large diamagnetic signal at 1.8 K confirms the bulk superconductivity. Figure 3(c) shows the suppression of T_c with the increase of the external magnetic field. The upper critical field, μ_0H_{c2}, is determined using the point where $\rho = 0$ on the resistivity transition curve, and plots of $\mu_0H_{c2}(T)$ are depicted in Fig. 3(e). A simple estimation of the $\mu_0H_{c2}(0)$ from the Ginzburg-Landau (GL) formula [52] is

$$\mu_0H_{c2}(T) = \mu_0H_{c2}(0)\frac{1-t^2}{1+t^2}, \tag{1}$$

where t = T/T_c, which gives an upper critical field of 5.40 T. The coherence length ξ can be acquired from the Ginzburg-Landau equation

$$\mu_0H_{c2} = \frac{\Phi}{2\pi\xi^2}, \tag{2}$$
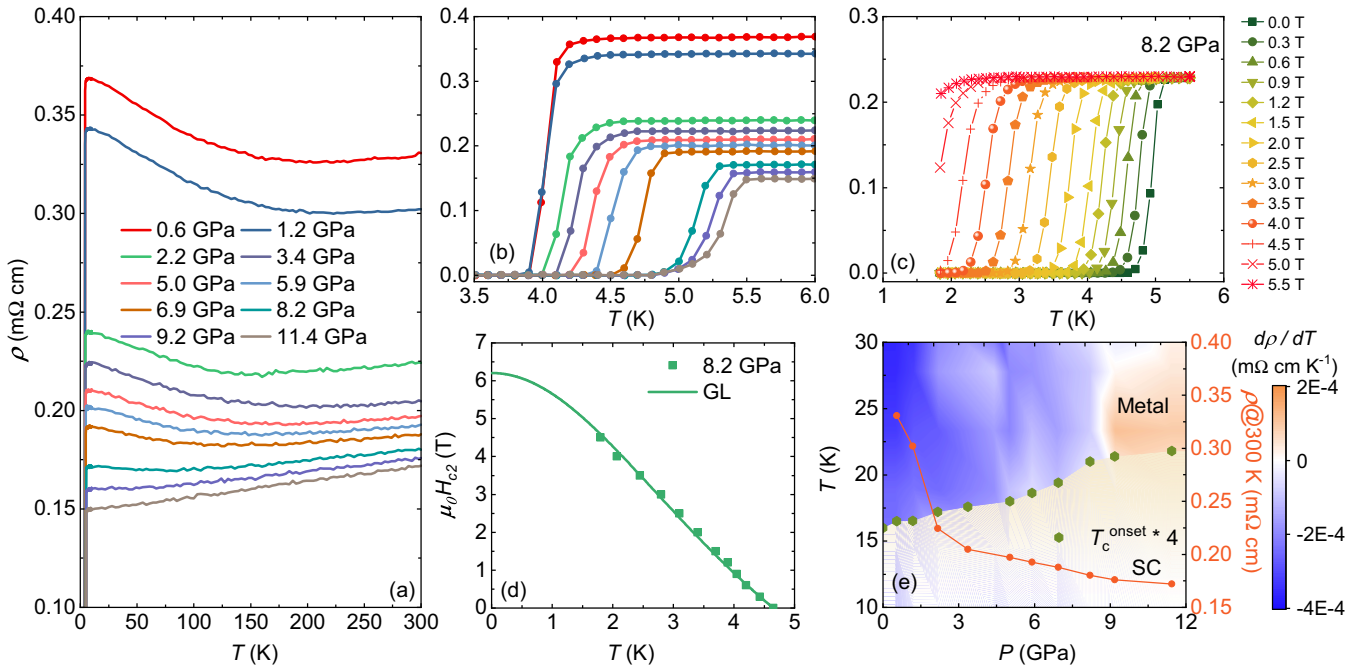
FIG. 4. Characterization of the superconducting transition of $Lu_5Rh_6Sn_{18}$ at various pressures. (a) Resistivity toward temperature obtained from the measurements in the pressure between 0.6 and 11.4 GPa, from 1.8 to 300 K. (b) Details of the resistivity at low temperatures for the data in (a), clearly indicating the impact of pressure on the resistivity through the superconducting transition and the preservation of the zero-resistance state. (c) Magnetic field dependence of the superconducting transition in $Lu_5Rh_6Sn_{18}$ at 8.2 GPa. (d) μ_0H_{c2} as a function of temperature. The solid line represents the Ginzburg-Landau fits. (e) Phase diagram of $Lu_5Rh_6Sn_{18}$. The red dots show the variation in resistivity with pressure at 300 K. Green hexagon represents superconducting T_c. The background represents the dependence of $d\rho/dT$ from 10 to 30 K at different pressures.

where Φ is the magnetic flux unit. By using $\mu_0 H_{c2}(0) = 5.40$ T, the calculated ξ should be 7.81 nm. The magnetization versus external field over a range of temperatures below T_c is presented in Fig. 3(d). The field deviating from a linear curve of full Meissner effect was deemed as the lower critical field $\mu_0 H_{c1}$ at each temperature and is summarized in Fig. 3(f). $\mu_0 H_{c1}(0)$ is found to be 4.14 mT by using the Ginzburg-Landau formula:

$$\mu_0 H_{c1}(T) = \mu_0 H_{c1}(0)\left[1 - \left(\frac{T}{T_c}\right)^2\right]. \qquad (3)$$

By using the formula [53]

$$\mu_0 H_{c1} = \frac{\Phi}{4\pi\lambda^2}\ln\left(1 + \sqrt{2}\frac{\lambda}{\xi}\right), \qquad (4)$$

we get the penetration depth $\lambda = 415$ nm. The calculated GL parameter of $\kappa = \lambda/\xi \sim 53.14$ confirms the type-II superconductivity in $Lu_5Rh_6Sn_{18}$. The thermodynamic critical fields $\mu_0 H_c(0)$ can be obtained by $\mu_0 H_{c2}(0)/\sqrt{2}\kappa$, and all the physical parameters are summarized in Table III.

In order to determine the pressure coefficient of T_c in $Lu_5Rh_6Sn_{18}$, we measured the electrical resistivity $\rho(T)$ of $Lu_5Rh_6Sn_{18}$ at various pressures. Figure 4(a) shows the typical $\rho(T)$ curves of $Lu_5Rh_6Sn_{18}$ for pressures up to 11.4 GPa. Increasing pressure induces a continuous suppression of the overall magnitude of ρ. At lower temperature the upturn of $\rho(T)$ fades away gradually and the semimetallic behavior is being suppressed by the application of pressure. Above 8.2 GPa, the $\rho(T)$ of $Lu_5Rh_6Sn_{18}$ exhibits typical metallic behavior. This is similar to the metallic behavior observed in $Y_5Rh_6Sn_{18}$ doped with La or Ti over the whole temperature range [55]. The band-structure calculations confirm the d-band character of the conduction electrons, which dominate the DOS at Fermi level [38,56,57]. The enhancement of the metallicity is likely attributed to the pressure of the increased Coulomb interaction between the d electrons of the transition metal, which dominate the field-dependent electronic transport in these materials [56]. Figure 4(b) shows the effect of pressure on the resistivity during the superconducting transition. T_c increases with pressure, and a maximum T_c^{onset} of 5.50 K is attained at 11.4 GPa, revealing a positive pressure coefficient of T_c. An overall increment rate of $dT_c/dP = 0.13$ K GPa^{-1} is shown in $Lu_5Rh_6Sn_{18}$ single crystals, which is comparable with other similar cage compounds [31,56]. Figure 4(c) demonstrates that the resistivity drop is continuously suppressed with increasing magnetic field. The value of $\mu_0 H_{c2}(0)$ was estimated to be 6.20 T at 8.2 GPa [Fig. 4(d)], which yields a coherence length ξ of 7.29 nm. The pressure dependence of T_c for $Lu_5Rh_6Sn_{18}$ is summarized in Fig. 4(e). Here the resistivity values at 300 K in different pressures are also shown. T_c increases with pressure and tends to saturate at pressures where the temperature dependence of the resistivity changes from a semimetal behavior to that of a normal metal. The coincidence of the pressure-induced metallicity and enhancement of T_c suggests a competitive correlation of superconductivity and the semimetal state.

To further identify the structural stability of $Lu_5Rh_6Sn_{18}$, we performed *in situ* high-pressure XRD measurements. Figure 5(a) illustrates the high-pressure synchrotron XRD
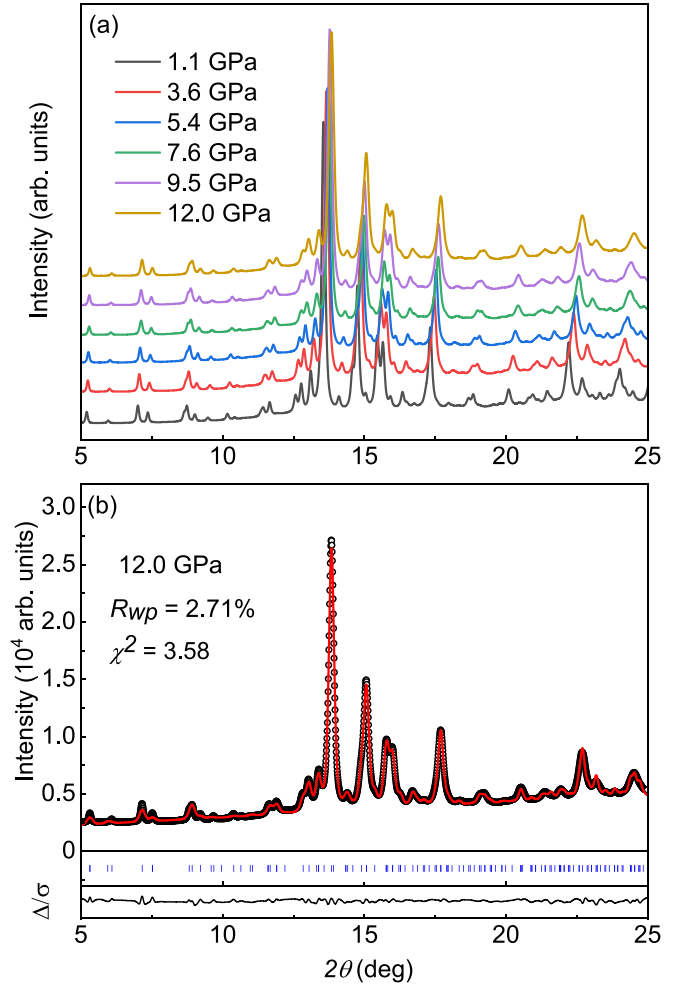
FIG. 5. (a) Powder XRD patterns of $Lu_5Rh_6Sn_{18}$ at various pressures up to 12.0 GPa. (b) XRD pattern together with the Rietveld refinement results at 12.0 GPa.

patterns of $Lu_5Rh_6Sn_{18}$ measured at room temperature and pressures up to 12.0 GPa. These patterns have been adjusted vertically for better data presentation. A representative refinement obtained at 12.0 GPa is displayed in Fig. 5(b). All the Bragg reflections can be refined by using the space group $I4_1/acd$ as the initial model. As shown in Fig. S4 in the Supplemental Material [43], both the a axis and c axis lattice parameters decrease with increasing pressure. A third-order Birch-Murnaghan equation of state [58] was used to fit the measured pressure-volume (P-V) data for $Lu_5Rh_6Sn_{18}$. The equation is given by

$$P(V) = \frac{3B_0}{2}\left[\left(\frac{V_0}{V}\right)^{7/3} - \left(\frac{V_0}{V}\right)^{5/3}\right]$$
$$\times\left\{1 + \frac{3}{4}(B_0' - 4)\left[\left(\frac{V_0}{V}\right)^{2/3} - 1\right]\right\}, \qquad (5)$$

where B_0 is the bulk modulus at ambient pressure, B_0' is the pressure derivative of B_0, and V_0 is the volume at ambient pressure. The obtained bulk modulus B_0 is 137.43 GPa with $V_0 = 5120$ Å^3. Our synchrotron diffraction indicates that the
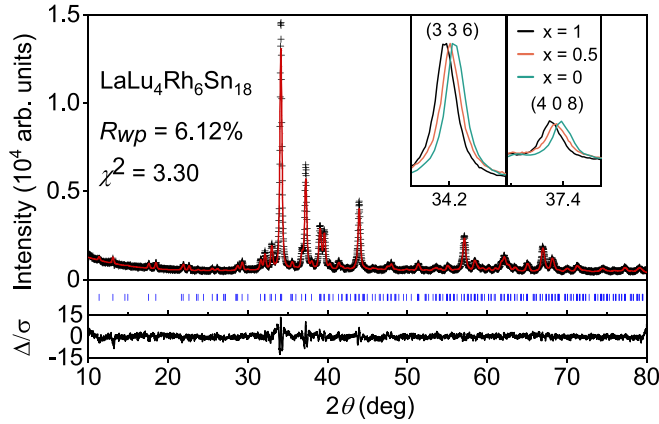
FIG. 6. Powder XRD pattern of LaLu$_4$Rh$_6$Sn$_{18}$. The insets show the appearance of the (3 3 6) and (4 0 8) reflection of the $x = 0$, 0.5, and 1 samples.

structure of Lu$_5$Rh$_6$Sn$_{18}$ is robust until 12.0 GPa and rules out the possibility of any structural phase transition. This finding indicates that the enhanced superconductivity under pressure originates from the pristine tetragonal phase.

Our high-pressure transport measurements demonstrate that lattice shrinkage is beneficial for improving superconductivity in Lu$_5$Rh$_6$Sn$_{18}$. To verify this scenario, we induce negative pressure by substituting the larger ion on the Lu site. Since La atoms have a relatively larger ionic radius, we chose La as the chemical dopant and grew a series of

TABLE IV. Chemical composition, lattice constants, and volume (V) of La$_x$Lu$_{5-x}$Rh$_6$Sn$_{18}$.

x	La:Lu:Rh:Sn	a, c (Å)	V (Å^3)
0	0.00 : 3.84 : 6.00 : 18.12	13.6829(3), 27.3503(9)	5120(3)
0.5	0.83 : 2.62 : 6.00 : 16.68	13.7095(5), 27.3885(11)	5148(5)
1	0.97 : 2.88 : 6.00 : 16.53	13.7143(12), 27.404(4)	5154(9)

La$_x$Lu$_{5-x}$Rh$_6$Sn$_{18}$ ($x = 0.5$ and 1) single crystals. From the EDS analysis (Fig. S2 in the Supplemental Material [43]), we indeed found the doping elements, i.e., La, in our single crystals. The powder XRD patterns of La$_x$Lu$_{1-x}$Rh$_6$Sn$_{18}$ ($x = 0.5$ and 1) (Figs. S4 and 6) show that all of the peaks can be well refined with the $I4_1/acd$ space group without any impurity phases. As shown in the insets of Fig. 6, the typical peaks of La-doped samples shift to lower angles, suggesting a lattice expansion. Details of the lattice constants are given in Table IV. The evolution of crystal lattices together with the EDS results demonstrates the successful chemical substitution in La$_x$Lu$_{5-x}$Rh$_6$Sn$_{18}$.

Figure 7(a) shows the resistivity $\rho(T)$ of the La$_x$Lu$_{5-x}$Rh$_6$Sn$_{18}$ ($x = 0.5$ and 1) single crystals. The doping of La does not enhance the metallicity; meanwhile, the superconducting transition temperature is suppressed to $T_c^{\text{onset}} = 3.83$ and 3.72 K for $x = 0.5$ and 1, respectively. The temperature dependence of the magnetic susceptibility is shown in Fig. 7(b) for both ZFC and FC conditions in an applied magnetic field of 10 Oe. The sharp superconducting
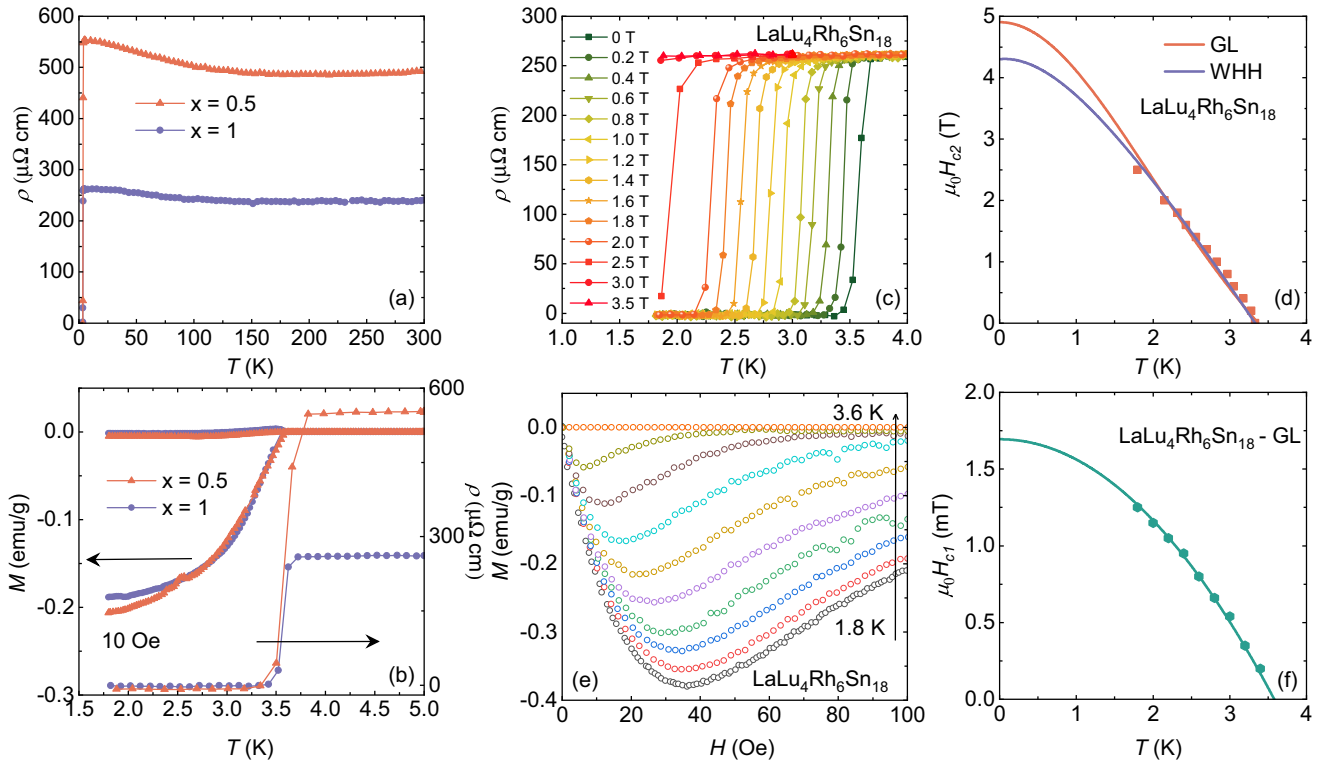
FIG. 7. (a) Resistivity of La$_x$Lu$_{5-x}$Rh$_6$Sn$_{18}$ ($x = 0.5$ and 1) in zero field from 1.8 to 300 K. (b) Superconducting transitions at low temperatures and the dc magnetic susceptibility in ZFC and FC conditions. (c) Electrical resistivity at various applied magnetic fields for LaLu$_4$Rh$_6$Sn$_{18}$. (d) Field dependence of the magnetization $M(H)$ of LaLu$_4$Rh$_6$Sn$_{18}$ at different temperatures below T_c. (e), (f) Temperature dependence of $\mu_0 H_{c2}$ and $\mu_0 H_{c1}$ for LaLu$_4$Rh$_6$Sn$_{18}$.
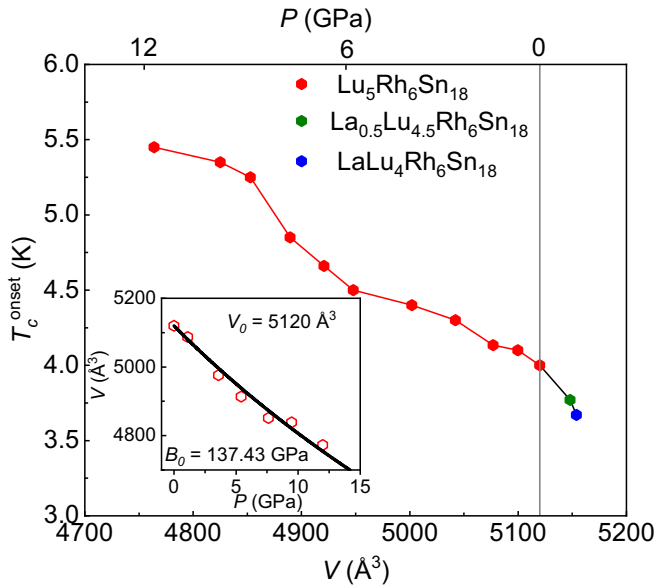
FIG. 8. T_c as a function of volume of $La_xLu_{5-x}Rh_6Sn_{18}$ ($x = 0$, 0.5, 1). Red points correspond to T_c^{onset} in the context of our high-pressure studies of $Lu_5Rh_6Sn_{18}$. The inset shows the unit-cell volume of $Lu_5Rh_6Sn_{18}$ up to around 12.0 GPa as a function of pressure. Black line represents the fitting result.

transition is observed in both samples with the onset of diamagnetism occurring at $T_c^{mag} = 3.63$ and 3.58 K for $x = 0.5$ and 1, respectively. We also performed the field dependence of $\rho(T)$ and $M(H)$ measurements for $LaLu_4Rh_6Sn_{18}$ as shown in Figs. 7(c) and 7(e). The values of $\mu_0H_{c2}(0)$ and $\mu_0H_{c1}(0)$ are estimated to be 4.30 T and 1.68 mT, respectively. Here, the temperature dependencies of μ_0H_{c2} are derived from Eq. (1) shown in Fig. 7(d). We tried to use the conventional Werthamer-Helfand-Hohenberg (WHH) formula to fit our data:

$$\mu_0H_{c2}(T) = -0.693T_c\frac{d\mu_0H_{c2}}{dT}|_{T=T_c}. \quad (6)$$

The slope $dH_{c2}(T)/dT = -1.86$ T/K for the $x = 1$ compound. $\mu_0H_{c2}(0)$ is estimated to be 4.30 T using the WHH formula. The details of the superconducting parameters are also summarized in Table III.

IV. DISCUSSION

At last, we discuss the effect of pressure on the superconductivity in $Lu_5Rh_6Sn_{18}$. Figure 8 plots the T_c^{onset} of $La_xLu_{5-x}Rh_6Sn_{18}$ ($x = 0$, 0.5, 1) as a function of the unit-cell

volume. It is clear to see the positive correlation between T_c and lattice volume in $La_xLu_{5-x}Rh_6Sn_{18}$. Application of high pressure is found to enhance both the metallicity and the superconducting transition temperature. Recently, high-pressure Raman spectrum measurements in the isostructural compound $Sc_5Rh_6Sn_{18}$ have shown that there is no pressure-induced phonon softening linked to cage shrinkage but a normal linear increase in the phonon mode frequencies [31]. Therefore, the improvement of T_c in $Lu_5Rh_6Sn_{18}$ under pressure can be attributed to an enhancement in DOS at the Fermi level. On the other hand, the introduction of La into $Lu_5Rh_6Sn_{18}$ induced a negative chemical pressure, which reasonably plays the opposite effect. In addition, La is larger than Lu, so the substitution of La ions would result in harmonic vibrations in $La_xLu_{5-x}Rh_6Sn_{18}$. Therefore the weakening of anharmonic rattling modes is detrimental to superconductivity [9,12,59]. It should be mentioned that the suppression of superconductivity in La-doped $Lu_5Rh_6Sn_{18}$ is contrary to the behavior observed in isostructural compounds [49,55,56], where local atomic disorder leads to an abnormal increase in the superconducting transition temperature T_c. Systematic studies from both experimental and theoretical perspectives are needed to understand the evolution of superconductivity in similar structures with various rare-earth atoms.

V. CONCLUSIONS

In summary, we systematically investigate the evolution of superconductivity in $Lu_5Rh_6Sn_{18}$ by applying physical pressure and chemical pressure. Application of pressure effectively improves both the metallic state and the superconductivity in $Lu_5Rh_6Sn_{18}$. The high-pressure XRD data revealed that the cage structure was stable without any structural phase transition up to ∼12.0 GPa. On the other hand, T_c was suppressed when negative chemical pressure was induced. Our results indicate the positive correlation between T_c and lattice volume in $La_xLu_{5-x}Rh_6Sn_{18}$, which will provide critical insight in similar caged superconductors.

[1] F. M. Grosche, H. Q. Yuan, W. Carrillo-Cabrera, S. Paschen, C. Langhammer, F. Kromer, G. Sparn, M. Baenitz, Y. Grin, and F. Steglich, Superconductivity in the filled cage compounds Ba_6Ge_{25} and $Ba_4Na_2Ge_{25}$, Phys. Rev. Lett. **87**, 247003 (2001).

[2] Z. Hiroi, J.-i. Yamaura, and K. Hattori, Rattling good superconductor: β-Pyrochlore oxides AOs_2O_6, J. Phys. Soc. Jpn. **81**, 011012 (2012).

[3] Y. Zhao, J. Deng, A. Bhattacharyya, D. T. Adroja, P. K. Biswas, L. L. Gao, W. Z. Cao, C. H. Li, C. Y. Pei, T. P. Ying *et al.*, Superconductivity in the layered cage compound $Ba_3Rh_4Ge_{16}$, Chin. Phys. Lett. **38**, 127402 (2021).

[4] C. W. Myles, K. Biswas, and E. Nenghabi, Rattling "guest" impurities in Si and Ge clathrate semiconductors, Phys. B: Condens. Matter **401-402**, 695 (2007).

[5] A. Maisuradze, W. Schnelle, R. Khasanov, R. Gumeniuk, M. Nicklas, H. Rosner, A. Leithe-Jasper, Y. Grin, A. Amato, and P. Thalmeier, Evidence for time-reversal symmetry breaking in superconducting PrPt$_4$Ge$_{12}$, Phys. Rev. B **82**, 024524 (2010).

[6] N. Takeda and M. Ishikawa, Superconducting and magnetic properties of filled skutterudite compounds RERu$_4$Sb$_{12}$ (RE = La, Ce, Pr, Nd, and Eu), J. Phys. Soc. Jpn. **69**, 868 (2000).

[7] I. Shirotani, Superconductivity of ternary metal compounds prepared at high pressures, Bull. Chem. Soc. Jpn. **76**, 1291 (2003).

[8] Y. P. Qi, H. C. Lei, J. G. Guo, W. J. Shi, B. H. Yan, C. Felser, and H. Hosono, Superconductivity in alkaline earth metal-filled skutterudites Ba$_x$Ir$_4$X$_{12}$ (X = As, P), J. Am. Chem. Soc. **139**, 8106 (2017).

[9] Y. Mizukami, M. Konczykowski, O. Tanaka, J. Juraszek, Z. Henkie, T. Cichorek, and T. Shibauchi, Suppression of anharmonic phonons and *s*-wave superconductivity by defects in the filled skutterudite LaRu$_4$As$_{12}$, Phys. Rev. Res. **2**, 043428 (2020).

[10] M. Brühwiler, S. M. Kazakov, J. Karpinski, and B. Batlogg, Mass enhancement, correlations, and strong-coupling superconductivity in the β-pyrochlore KOs$_2$O$_6$, Phys. Rev. B **73**, 094518 (2006).

[11] T. Terashima, S. Uji, Y. Nagao, J. Yamaura, Z. Hiroi, and H. Harima, Fermi surface in the superconducting β-pyrochlore oxide CsOs$_2$O$_6$, Phys. Rev. B **77**, 064509 (2008).

[12] Y. Shimono, T. Shibauchi, Y. Kasahara, T. Kato, K. Hashimoto, Y. Matsuda, J. Yamaura, Y. Nagao, and Z. Hiroi, Effects of rattling phonons on the dynamics of quasiparticle excitation in the β-pyrochlore KOs$_2$O$_6$ superconductor, Phys. Rev. Lett. **98**, 257004 (2007).

[13] H. Sugawara, T. D. Matsuda, K. Abe, Y. Aoki, H. Sato, S. Nojiri, Y. Inada, R. Settai, and Y. Ōnuki, Exotic heavy-fermion state in the filled skutterudite PrFe$_4$P$_{12}$ uncovered by the de Haas–van Alphen effect, Phys. Rev. B **66**, 134411 (2002).

[14] K. Iwasa, L. Hao, K. Kuwahara, M. Kohgi, S. R. Saha, H. Sugawara, Y. Aoki, H. Sato, T. Tayama, and T. Sakakibara, Evolution of 4*f* electron states in the metal-insulator transition of PrRu$_4$P$_{12}$, Phys. Rev. B **72**, 024414 (2005).

[15] Y. Kuramoto, H. Kusunose, and A. Kiss, Multipole orders and fluctuations in strongly correlated electron systems, J. Phys. Soc. Jpn. **78**, 072001 (2009).

[16] J. G. Guo, J. Yamaura, H. C. Lei, S. Matsuishi, Y. P. Qi, and H. Hosono, Superconductivity in Ba$_{n+2}$Ir$_{4n}$Ge$_{12+n}$ (n = 1, 2) with cage structure and softening of low-lying localized mode, Phys. Rev. B **88**, 140507(R) (2013).

[17] G. Espinosa, A. Cooper, and H. Barz, Isomorphs of the superconducting/magnetic ternary stannides, Mater. Res. Bull. **17**, 963 (1982).

[18] G. P. Espinosa, A. S. Cooper, H. Barz, and J. P. Remeika, Crystal chemistry, growth and reentrant behavior of additional superconducting/magnetic stannides, Mater. Res. Bull. **15**, 1635 (1980).

[19] G. Espinosa, Crystal growth and crystal-chemical investigation of systems containing new superconducting and/or magnetic ternary stannides, Mater. Res. Bull. **15**, 791 (1980).

[20] A. Bhattacharyya, D. T. Adroja, N. Kase, A. D. Hillier, A. M. Strydom, and J. Akimitsu, Unconventional superconductivity in the cage-type compound Sc$_5$Rh$_6$Sn$_{18}$, Phys. Rev. B **98**, 024511 (2018).

[21] A. Bhattacharyya, D. T. Adroja, J. Quintanilla, A. D. Hillier, N. Kase, A. M. Strydom, and J. Akimitsu, Broken time-reversal symmetry probed by muon spin relaxation in the caged type superconductor Lu$_5$Rh$_6$Sn$_{18}$, Phys. Rev. B **91**, 060503(R) (2015).

[22] Z. Zhang, Y. Xu, C. N. Kuo, X. C. Hong, M. X. Wang, P. L. Cai, J. K. Dong, C. S. Lue, and S. Y. Li, Nodeless superconducting gap in the caged-type superconductors Y$_5$Rh$_6$Sn$_{18}$ and Lu$_5$Rh$_6$Sn$_{18}$, Supercond. Sci. Technol. **28**, 105008 (2015).

[23] M. Feig, W. Schnelle, A. Maisuradze, A. Amon, C. Baines, M. Nicklas, S. Seiro, L. Howald, R. Khasanov, A. Leithe-Jasper *et al.*, Conventional isotropic *s*-wave superconductivity with strong electron-phonon coupling in Sc$_5$Rh$_6$Sn$_{18}$, Phys. Rev. B **102**, 024508 (2020).

[24] A. Bhattacharyya, D. Adroja, N. Kase, A. Hillier, J. Akimitsu, and A. Strydom, Unconventional superconductivity in Y$_5$Rh$_6$Sn$_{18}$ probed by muon spin relaxation, Sci. Rep. **5**, 12926 (2015).

[25] A. Rojek, C. Sułkowski, and K. Rogacki, Superconductivity and magnetism of TmRh$_{1.3}$Sn$_{4.0}$ single crystals, Physica C **223**, 111 (1994).

[26] J. Hodeau, M. Marezio, and J. Remeika, The structure of [Er(1)$_{1-x}$, Sn(1)$_x$]Er(2)$_4$Rh$_6$Sn(2)$_4$Sn(3)$_{12}$Sn(4)$_2$, A reentrant superconductor, Acta Crystallogr. Sect. B: Struct. Sci. **40**, 26 (1984).

[27] C. Pei, T. Ying, Y. Zhao, L. Gao, W. Cao, C. Li, H. Hosono, and Y. Qi, Pressure-induced reemergence of superconductivity in BaIr$_2$Ge$_7$ and Ba$_3$Ir$_4$Ge$_{16}$ with cage structures, Matter Radiat. Extremes **7**, 038404 (2022).

[28] C. Y. Pei, T. P. Ying, Q. H. Zhang, X. X. Wu, T. X. Yu, Y. Zhao, L. L. Gao, C. H. Li, W. Z. Cao, Q. Zhang *et al.*, Caging-Pnictogen-induced superconductivity in skutterudites IrX$_3$ (X = As, P), J. Am. Chem. Soc. **144**, 6208 (2022).

[29] A. Slebarski, M. Fijalkowski, M. M. Maska, M. Mierzejewski, B. D. White, and M. B. Maple, Superconductivity of La$_3$Co$_4$Sn$_{13}$ and La$_3$Rh$_4$Sn$_{13}$: A comparative study, Phys. Rev. B **89**, 125111 (2014).

[30] A. Ślebarski, M. M. Maśka, M. Fijałkowski, C. A. McElroy, and M. B. Maple, Superconductivity in the presence of disorder in skutterudite-related La$_3$Co$_4$Sn$_{13}$ and La$_3$Ru$_4$Sn$_{13}$ compounds: Electrical transport and magnetic studies, J. Alloys Compd. **646**, 866 (2015).

[31] G. Lingannan, B. Joseph, M. Sundaramoorthy, C. N. Kuo, C. S. Lue, and S. Arumugam, Pressure-enhanced superconductivity in cage-type quasiskutterudite Sc$_5$Rh$_6$Sn$_{18}$ single crystal, J. Phys.: Condens. Matter **34**, 245601 (2022).

[32] J. Remeika, G. Espinosa, A. Cooper, H. Barz, J. Rowell, D. McWhan, J. Vandenberg, D. Moncton, Z. Fisk, and L. Woolf, A new family of ternary intermetallic superconducting/magnetic stannides, Solid State Commun. **34**, 923 (1980).

[33] B. H. Toby and R. B. Von Dreele, GSAS-II: The genesis of a modern open-source all purpose crystallography software package, J. Appl. Crystallogr. **46**, 544 (2013).

[34] Q. Wang, P. F. Kong, W. J. Shi, C. Y. Pei, C. H. P. Wen, L. L. Gao, Y. Zhao, Q. W. Yin, Y. S. Wu, G. Li *et al.*, Charge density wave orders and enhanced superconductivity under pressure in the kagome metal CsV$_3$Sb$_5$, Adv. Mater. **33**, 2102813 (2021).

[35] C. Pei, J. Zhang, C. Gong, Q. Wang, L. Gao, Y. Zhao, S. Tian, W. Cao, C. Li, Z.-Y. Lu *et al.*, Distinct superconducting behaviors of pressurized WB$_2$ and ReB$_2$ with different local B layers, Sci. China Phys. Mech. Astron. **65**, 287412 (2022).

[36] C. Pei, J. Zhang, Q. Wang, Y. Zhao, L. Gao, C. Gong, S. Tian, R. Luo, M. Li, W. Yang *et al.*, Pressure-induced superconductivity at 32 K in MoB_2, Natl. Sci. Rev. **10**, nwad034 (2023).

[37] H. K. Mao, J. Xu, and P. M. Bell, Calibration of the ruby pressure gauge to 800 kbar under quasi-hydrostatic conditions, J. Geophys. Res. **91**, 4673 (1986).

[38] A. Wang, Z. Y. Nie, F. Du, G. M. Pang, N. Kase, J. Akimitsu, Y. Chen, M. J. Gutmann, D. T. Adroja, R. S. Perry *et al.*, Nodeless superconductivity in $Lu_{5-x}Rh_6Sn_{18+x}$ with broken time reversal symmetry, Phys. Rev. B **103**, 024503 (2021).

[39] O. V. Dolomanov, L. J. Bourhis, R. J. Gildea, J. A. K. Howard, and H. Puschmann, *OLEX2*: A complete structure solution, refinement and analysis program, J. Appl. Crystallogr. **42**, 339 (2009).

[40] A. A. Sarjeant, Structure solution and refinement with Olex2: A guide for chem 435 students, http://imserc.northwestern.edu/downloads/crystallography-Olex2-NU.pdf (2015).

[41] G. M. Sheldrick, SHELXT - Integrated space-group and crystal-structure determination, Acta Crystallogr. Sect. A **71**, 3 (2015).

[42] G. M. Sheldrick, Crystal structure refinement with SHELXL, Acta Crystallogr. Sect. C-Struct. Chem. **71**, 3 (2015).

[43] See Supplemental Material at http://link.aps.org/supplemental/10.1103/PhysRevB.109.075202 for single and powder XRD results, EDS, and relationship between lattice parameters of $Lu_5Rh_6Sn_{18}$ and pressures.

[44] M. Feig, L. Akselrud, W. Schnelle, V. Dyadkin, D. Chernyshov, A. Ormeci, P. Simon, A. Leithe-Jasper, and R. Gumeniuk, Crystal structure, chemical bonding, and electrical and thermal transport in $Sc_5Rh_6Sn_{18}$, J. Chem. Soc. Dalton Trans. **49**, 6832 (2020).

[45] V. Levytskyi, W. Carrillo-Cabrera, L. Akselrud, B. Kundys, A. Leithe-Jasper, and R. Gumeniuk, Superconductivity of structurally disordered $Y_5Ir_6Sn_{18}$, J. Chem. Soc., Dalton Trans. **51**, 10036 (2022).

[46] I. W. H. Oswald, B. K. Rai, G. T. McCandless, E. Morosan, and J. Y. Chan, The proof is in the powder: Revealing structural peculiarities in the $Yb_3Rh_4Sn_{13}$ structure type, CrystEngComm **19**, 3381 (2017).

[47] S. Miraglia, J. L. Hodeau, F. de Bergevin, M. Marezio, and G. P. Espinosa, Structural studies by electron and X-ray diffraction of the disordered phases II': $(Sn_{1-x}Tb_x)Tb_4Rh_6Sn_{18}$ and $(Sn_{1-x}Dy_x)Dy_4Os_6Sn_{18}$, Acta Crystallogr. Sect. B: Struct. Sci. **43**, 76 (1987).

[48] C.-W. Wang, S. K. Karna, S.-i. Yano, C.-H. Lee, M. Avdeev, C. S. Lue, and C. N. Kuo, Magnetic properties and noncollinear spin structure of the tin-rich stannide $Ho_5Co_6Sn_{18}$, Phys. Rev. B **105**, 104429 (2022).

[49] A. Ślebarski, M. Fijałkowski, M. M. Maśka, J. Deniszczyk, P. Zajdel, B. Trump, and A. Yakovenko, Enhancing superconductivity of $Lu_5Rh_6Sn_{18}$ by atomic disorder, Phys. Rev. B **103**, 155133 (2021).

[50] N. F. Mott, The effect of electron interaction on variable-range hopping, Philos. Mag. **34**, 643 (1976).

[51] B. Raquet, M. N. Baibich, J. M. Broto, H. Rakoto, S. Lambert, and A. Maignan, Hopping conductivity in one-dimensional $Ca_3Co_2O_6$ single crystals, Phys. Rev. B **65**, 104442 (2002).

[52] C. K. Jones, J. K. Hulm, and B. S. Chandrasekhar, Upper critical field of solid solution alloys of the transition elements, Rev. Mod. Phys. **36**, 74 (1964).

[53] E. F. Talantsev, Method to extracting the penetration field in superconductors from DC magnetization data, Rev. Sci. Instrum. **93**, 053912 (2022).

[54] J. Akimitsu, Towards higher-T_c superconductors, Proc. Jpn. Acad., Ser. B **95**, 321 (2019).

[55] M. Fijałkowski, M. M. Maśka, J. Deniszczyk, and A. Ślebarski, Magnetic field induced reentrance of superconductivity in the cage-type superconductor $Y_5Rh_6Sn_{18}$, Phys. Rev. B **104**, 165306 (2021).

[56] A. Ślebarski, M. Fijałkowski, P. Zajdel, M. M. Maśka, J. Deniszczyk, M. Zubko, O. Pavlosiuk, K. Sasmal, and M. B. Maple, Enhancing superconductivity of $Y_5Rh_6Sn_{18}$ by atomic disorder, Phys. Rev. B **102**, 054514 (2020).

[57] J. Deniszczyk and A. Slebarski, Band structure studies of the $R_5Rh_6Sn_{18}$ (R = Sc, Y, Lu) quasiskutteridite superconductors, Materials **15**, 2451 (2022).

[58] F. Birch, Finite elastic strain of cubic crystals, Phys. Rev. **71**, 809 (1947).

[59] M. J. Winiarski, B. Wiendlocha, M. Sternik, P. Wiśniewski, J. R. O'Brien, D. Kaczorowski, and T. Klimczuk, Rattling-enhanced superconductivity in MV_2Al_{20} (M = Sc, Lu, Y) intermetallic cage compounds, Phys. Rev. B **93**, 134507 (2016).